ARTICLE

Radiation effects on lithium metal batteries
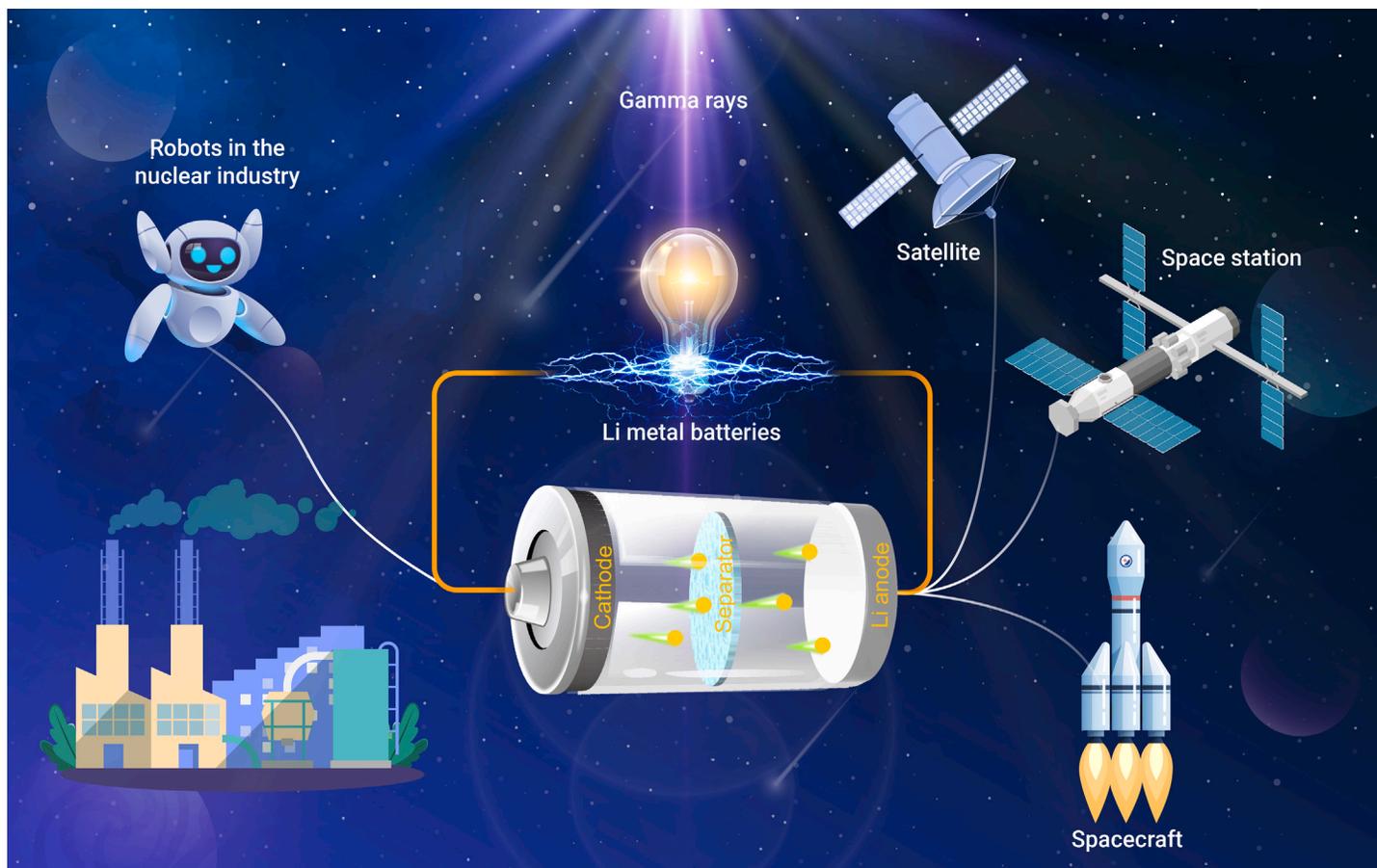
Yuliang Gao,[1,2] Fahong Qiao,[1] Weiping Hou,[2] Li Ma,[1] Nan Li,[1,3,*] Chao Shen,[1] Ting Jin,[1] and Keyu Xie[1,4,*]

*Correspondence: nan1li@polyu.edu.hk (N.L.); kyxie@nwpu.edu.cn (K.X.)

GRAPHICAL ABSTRACT

PUBLIC SUMMARY

- The effect of gamma rays on Li metal batteries is explored.

- Gamma rays deteriorate the electrochemical performance of Li metal batteries.

- The gamma radiation-induced failure mechanism of Li metal batteries is revealed.

- The irradiation tolerance of key battery materials is identified.

Radiation effects on lithium metal batteries

Yuliang Gao,[1,2] Fahong Qiao,[1] Weiping Hou,[2] Li Ma,[1] Nan Li,[1,3,*] Chao Shen,[1] Ting Jin,[1] and Keyu Xie[1,4,*]

[1]State Key Laboratory of Solidification Processing, Center for Nano Energy Materials, School of Materials Science and Engineering, Northwestern Polytechnical University and Shaanxi Joint Laboratory of Graphene (NPU), Xi'an 710072, China

[2]School of Chemistry and Chemical Engineering, Inner Mongolia University, Hohhot 010021, China

[3]Department of Applied Physics, The Hong Kong Polytechnic University, Hong Kong 999077, China

[4]Institute of Clean Energy, Yangtze River Delta Research Institute, Northwestern Polytechnical University, Xi'an 710072, China

*Correspondence: nan1li@polyu.edu.hk (N.L.); kyxie@nwpu.edu.cn (K.X.)

The radiation tolerance of energy storage batteries is a crucial index for universe exploration or nuclear rescue work, but there is no thorough investigation of Li metal batteries. Here, we systematically explore the energy storage behavior of Li metal batteries under gamma rays. Degradation of the performance of Li metal batteries under gamma radiation is linked to the active materials of the cathode, electrolyte, binder, and electrode interface. Specifically, gamma radiation triggers cation mixing in the cathode active material, which results in poor polarization and capacity. Ionization of solvent molecules in the electrolyte promotes decomposition of LiPF$_6$ along with its decomposition, and molecule chain breaking and cross-linking weaken the bonding ability of the binder, causing electrode cracking and reduced active material utilization. Additionally, deterioration of the electrode interface accelerates degradation of the Li metal anode and increases cell polarization, hastening the demise of Li metal batteries even more. This work provides significant theoretical and technical evidence for development of Li batteries in radiation environments.

INTRODUCTION

Exploring new energy technologies is now essential because of the rising energy crisis and environmental pollution, and it will be crucial for the global energy transition to support the electrification of various industrially derived equipment. Li-ion batteries are some of the most widely utilized types of rechargeable batteries and are frequently employed in common applications like electric vehicles, smart grids, and electronic devices.[1,2] Additionally, they have crucial uses under harsh conditions, such as unmanned vehicles conducting surveys, rescue operations in radioactive environments, or vehicles and probes for extraterrestrial research. Current Li-ion batteries, however, are no longer able to supply the electricity needed by practical electric devices because of the low theoretical capacity of a graphite anode, so there is an urgent need to develop new high-energy-density batteries. Compared with advanced Li-ion batteries (<300 Wh kg^{-1}), Li metal batteries have an energy density several times higher (such as the theoretical energy density of 2,600 Wh kg^{-1} for Li-sulfur batteries) and offer a workable remedy for the energy storage shortage of the electric drive equipment.[3–5]

Up to now, development of Li metal batteries has concentrated on modification of each essential component, including separator modification,[6–8] electrolyte optimization,[9–11] Li electrode design,[12–14] and protective layer construction.[15–17] However, the effects of the external physical environment the batteries may experience when in service are disregarded. We previously explored the effects of supergravity fields on Li metal batteries.[18] It was demonstrated that a supergravity field homogenizes Li deposition and stabilizes the solid electrolyte interface on the electrode surface, ultimately conferring enhanced cycling stability to Li metal batteries. Li metal batteries are also exposed to irradiation, like gamma rays, when serving in space and in the nuclear industry (Figure 1A).

Gamma rays have the strongest energy in the electromagnetic spectrum and the highest penetration ability.[19] The ionization and displacement effects resulting from the interaction of gamma rays with materials would trigger microscopic changes that contribute to alterations in the performance of the materials or devices.[20] Researchers have utilized the free radicals generated by ionization under gamma rays to promote cross-linking of molecules for high-performance materials.[21] Some scholars have also employed its ionizing effect to treat cancer and eliminate bacteria.[22–24] Besides the positive utilization of turning "waste into treasure," the effects of gamma radiation are more dominated by the performance deterioration of materials or devices. Gamma rays lower the spectral responsiveness, raise the dark current, and lengthen the response time of the silicon photodiode in the particular radiometer, and under extreme circumstances, they can harm or permanently destroy the detector.[25] Erbium-ytterbium co-doped gain fibers produce color centers in the gain fibers in a radiation environment, causing a large impact on the performance parameters of the amplifier, especially the output power characteristics.[26] Additionally, gamma radiation exposure can cause radiation damage to linear integrated circuits.[27] The US National Geophysical Data Center's statistics of in-orbit anomalies for 39 satellites operating in geosynchronous and quasi-synchronous orbit from 1971–1986 found that more than 70% of the failures were caused by space charged particle radiation.[28] Sorting out the effects of gamma radiation on equipment and its crucial components is crucial to advancing their uses under radiation conditions. The service behavior of Li metal batteries influences safe operation of the entire equipment as a potential power source for future space-related or nuclear sector rescue equipment. However, it is still unclear how gamma radiation would affect Li metal batteries.

Here, we explored the gamma radiation effect on Li metal batteries and revealed the corresponding mechanisms. First, the electrochemical performance of Li metal batteries under gamma radiation is assessed, and then the contribution of key battery components to performance deterioration is elucidated. On this basis, the mechanisms of gamma radiation-induced degradation and radiation tolerance of common cathode active materials (LiNi$_{0.8}$Co$_{0.1}$Mn$_{0.1}$O$_2$ [NCM811], LiFePO$_4$ [LFP], and LiCoO$_2$ [LCO]), binders (polyvinylidene fluoride [PVDF], polyacrylonitrile [PAN], polyethylene oxide [PEO], and carboxymethyl cellulose [CMC]), and electrolyte (LiPF$_6$- and LiBF$_4$-based electrolyte) are revealed, respectively. Further research is also being conducted on the interface chemistry of the cathode and anode of Li metal batteries exposed to gamma radiation. Finally, the electrochemical performance degradation mechanism of Li metal batteries in the presence of gamma radiation is presented. This work reveals the energy storage behavior of Li metal batteries exposed to gamma rays and provides clear directions for their subsequent improvement in radiation environment applications.

RESULTS AND DISCUSSION

Electrochemical performance of Li metal batteries under gamma radiation

To explore the impact of gamma radiation on the electrochemical performance of Li metal batteries, NCM811||Li, LFP||Li, and LCO||Li full cells were assembled separately. Co-60 was employed as the radiation source, and the cells or materials that received a dosage of 20 kGy were labeled (NCM811||Li)-20, (LFP||Li)-20, (LCO||Li)-20, NCM811-20, etc. Accordingly, the controls for no irradiation were (NCM811||Li)-0, (LFP||Li)-0, (LCO||Li)-0, NCM811-0, etc. Figure 1B displays the deterioration of the cycling performance of Li metal batteries under gamma radiation. After 350 cycles at 1 C, the capacity retention rates of (NCM811||Li)-20, (LFP||Li)-20, and (LCO||Li)-20 batteries were 57.7%, 69.6%, and 70.3%, while those of the controls were 76.6%, 90.9%, and 94.2%, respectively. Such extraordinary performance differences indicate a detrimental impact of gamma radiation on Li metal batteries.

The electrochemical performance of each key material (electrolyte, cathode active material, binder, conductive agent, Li metal, and separator) after gamma radiation was investigated separately to identify the causes. In comparison with Li metal batteries with standard electrolyte, the capacity retention rates of NCM811||Li-(electrolyte-20), LFP||Li-(electrolyte-20), and LCO||Li-(electrolyte-20) batteries decreased to 67.5%, 70.4%, and 77.7% after 350 cycles, as shown in
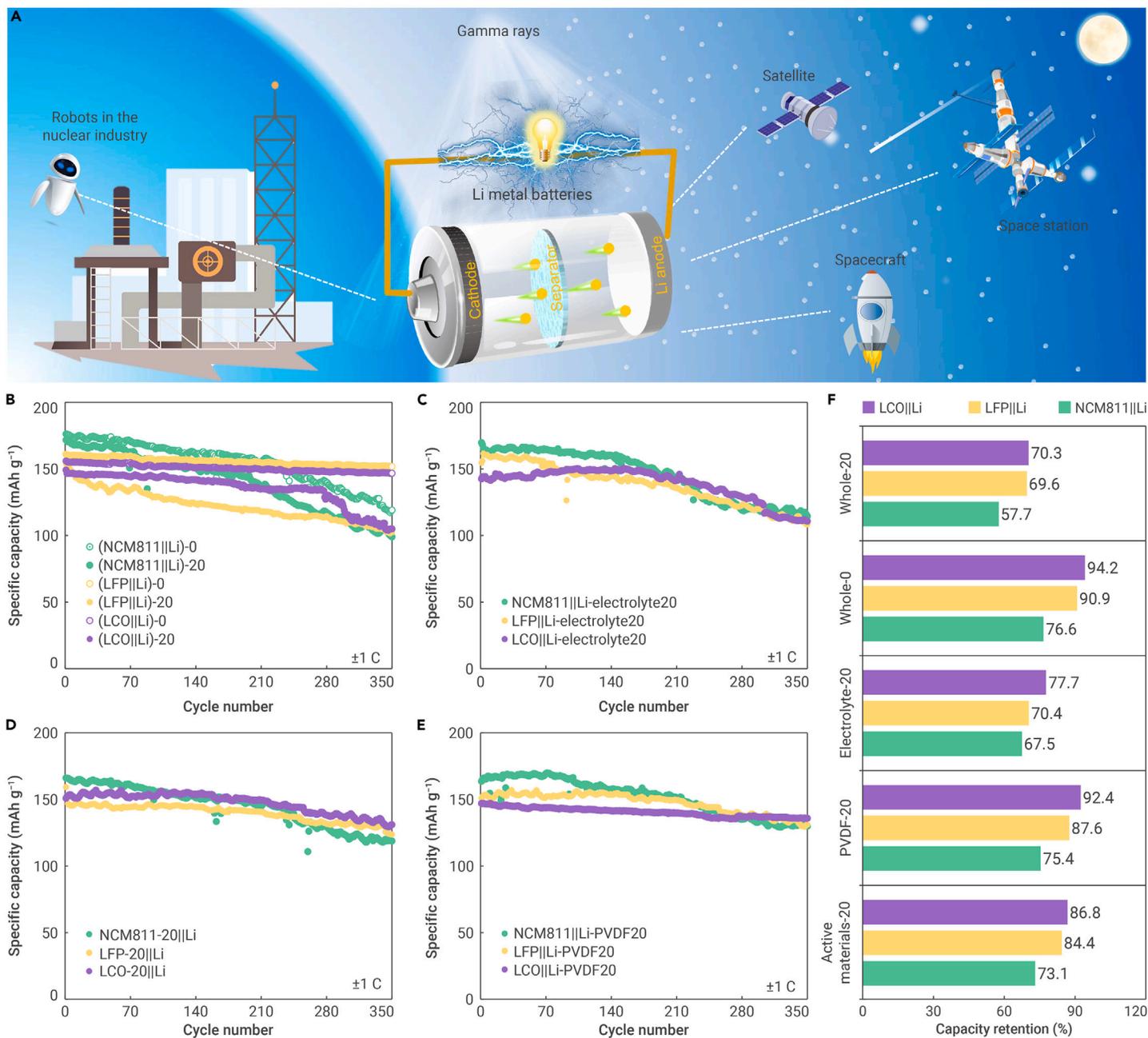
Figure 1. Potential applications of Li metal batteries and their electrochemical performance under gamma radiation (A) Potential application of Li metal batteries. (B–E) Cycling stability of Li metal batteries with three different cathodes (NCM811, LFP, and LCO) after radiation (20 kGy) (B) as well as irradiated electrolyte (C), cathode active materials (D), and PVDF(E). (F) Comparison of the capacity retention rates of the aforementioned Li metal batteries.

Figure 1C, demonstrating serious gamma radiation effects on the electrolyte. Also, gamma radiation has a potential impact on the three cathode active materials, with capacity retention rates of NCM811-20∥Li, LFP-20∥Li, and LCO-20∥Li batteries falling successively to 73.1%, 84.4%, and 86.8% after 350 cycles (Figure 1D). For monolithic materials (Li metal and Super P), X-ray diffraction (XRD) spectra and electrochemical performance measurements revealed negligible gamma radiation effects (Figures S1 and S2). Regarding the polypropylene separator, there was a slight change in the wettability of the electrolyte and the tensile strength of the separator after gamma radiation but no notable variations in its microporous structure and electrochemical performance; thus, its contribution to the electrochemical performance of Li metal batteries can be disregarded (Figure S3). Irradiated PVDF also triggered decreases in cell performance after 350 cycles, with capacity retention rates of 75.4%, 87.6%, and 92.4% for NCM811∥Li-(PVDF-20), LFP∥Li-(PVDF-20), and LCO∥Li-(PVDF-20), respectively (Figure 1E). The cathode active material, electrolyte, and binder are apparently associated with deterioration in the electrochemical performance of Li metal batteries when exposed to gamma radiation. Based on the difference in capacity

retention between the blank group ((NCM811∥Li)-0, (LFP∥Li)-0, and (LCO∥Li)-0) and batteries assembled with each irradiated material, it is clear that the electrolyte is the bulk of this failure, followed by the cathode active materials, and finally the binders (Figure 1F). NCM811∥Li batteries have the best tolerance to irradiation, with decreasing values of capacity retention following gamma irradiation for LFP∥Li, NCM811∥Li, and LCO∥Li batteries of 18.9%, 21.3%, and 23.9%, respectively.

Evaluation of electrolyte under gamma radiation

To elucidate the intrinsic mechanism of electrolyte-induced deterioration of battery performance under gamma radiation, the microscopic evolution of the electrolyte was explored. After gamma radiation, 1.0 M $LiPF_6$+ethylene carbonate(EC)/diethyl carbonate(DEC)/ethyl methyl carbonate(EMC) electrolyte shows no real-time color change but then evolves into a yellow-brown liquid after 30 days of placement, and the color deepens with increasing radiation dose (Figures 2A and S4). This shows that the decomposition of the electrolyte was initiated by gamma radiation, but the effect is not immediately apparent, only after
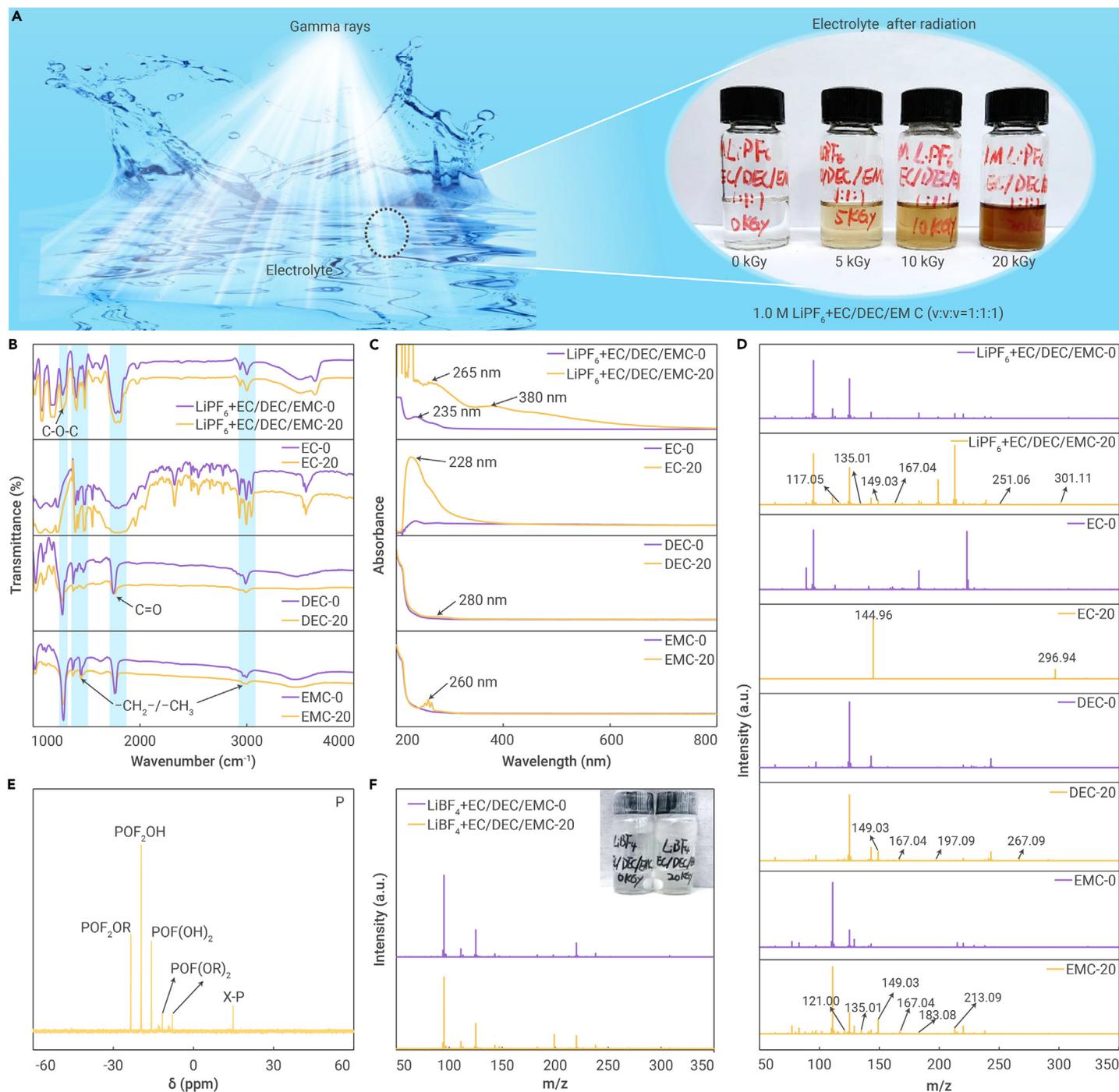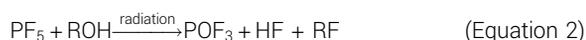
Figure 2. Evaluation of electrolyte under gamma radiation (A) Schematic of gamma-irradiated electrolyte and post-radiation optical photos. (B–D) FTIR (B), UV-vis (C), and HRMS (D) spectra of electrolytes and their solvent components before and after gamma irradiation. (E) ^{31}P NMR spectrum of the irradiated electrolyte. (F) HRMS spectra of LiBF$_4$-based electrolytes before and after gamma irradiation. The inset shows an optical photo of the electrolyte before (left) and after (right) gamma irradiation.

a certain time. Different dosages of LiPF$_6$ radiation were given individually to the irradiated solvent in an effort to identify the cause of the electrolyte disintegration. However, no notable change in the electrolyte's color was observed (Figures S5A and S5B). The structural and electrochemical properties of LiPF$_6$ were unaltered as well (Figures S5C and S5D). Gamma radiation was also applied to the solvents EC, DEC, EMC, and EC/DEC/EMC, but no discernible color was noticed. The electrolyte color comes out noticeably when irradiated LiPF$_6$ is added to EC/DEC/EMC and then deepens with increasing radiation dose, illustrating that the step-by-step decomposition of LiPF$_6$ by the radiated decomposed solvent becomes the prime reason for radiation-induced electrolyte discoloration (Figure S6).

The Fourier transform infrared (FTIR) spectra provide detailed information about the electrolyte's decomposition. The characteristic peaks of the electrolyte and solvent, such as $-CH_2/-CH_3$ (1,300–1,450 and 2,900–3,000 cm^{-1}), C=O

(1,750 cm^{-1}), and C$-$O$-$C (1,259 cm^{-1}),[29] became weak after radiation, as shown in Figure 2B, suggesting that the introduction of gamma rays sparked the decomposition reactions of the electrolyte and solvent molecules. The UV-visible (UV-vis) spectra show that the electrolyte emerged with a new absorption peak at 380 nm after gamma radiation, which corresponds to the phosphorus-containing colored decomposition products (Figure 2C). The absorption peak at 235 nm was redshifted to 265 nm, showing that the decomposition reaction increased the system conjugation degree. The decomposition impact of gamma radiation on the electrolyte was further supported by the fact that all EC, DEC, and EMC molecules displayed a new peak at wavelengths of 228, 280, and 260 nm, respectively. As is evident, radicals created during the gamma radiation-induced decomposition of solvent molecules increase system conjugation and trigger its combination with LiPF$_6$ to produce a series of products.

The decomposition products of the electrolyte after gamma radiation were examined using high-resolution mass spectrometry (HRMS). New peaks appeared in the electrolyte and solvents, as shown in Figure 2D, indicating formation of new decomposition products. We suggested potential breakdown products and included them in Tables S1 and S2 based on the molecular weight. The tables show that all new chemicals created by disintegration of the electrolyte under gamma radiation contain elemental phosphorus, which is exactly what causes the change of the electrolyte from colorless to yellow-brown. Because the majority of the breakdown products for EC are $POF_2C_2H_4OF$ (144.96) and $POF_2C_6H_9F_4O_4$ (296.94) after gamma irradiation, this suggests that the free radicals generated by EC molecules reacted preferentially with $LiPF_6$. Many of the same breakdown products for DEC and EMC were present before and after gamma radiation, demonstrating that the solvent molecule-produced free radicals reacted not just with $LiPF_6$ but also among themselves. Additionally, a comparative study discovered that the decomposition products of the mixed solvents were nearly identical to those of the single one. Examining the decomposition products of electrolyte also involved using NMR analyses (Figure 2E). The peaks at −14.9, −7.6 (−11.1), −15.6, −19.4, and −23.4 ppm in ^{31}P NMR correspond to X-P, $POF(OR)_2$, $POF(OH)_2$, POF_2OH, and POF_2OR, respectively (X refers to fragments containing the element C). The PF_6^-, $POF(OH)_2$, POF_2OR, and HF peaks appear at −77.1, −85.1, −86.7, and −156.5 ppm in ^{19}F NMR (Figure S7),[30] suggesting that $LiPF_6$ undergoes the following decomposition reactions:

$$LiPF_6 \xrightarrow{radiation} LiF + PF_5 \qquad \text{(Equation 1)}$$

$$PF_5 + ROH \xrightarrow{radiation} POF_3 + HF + RF \qquad \text{(Equation 2)}$$

$$POF_3 + H_2O \xrightarrow{radiation} POF(OH)_2 / POF_2OH + HF \qquad \text{(Equation 3)}$$

$$POF_3 + ROH \xrightarrow{radiation} POF_2OR / POF(OR)_2 + HF \qquad \text{(Equation 4)}$$

$$POF_3 + RCO_3R \xrightarrow{radiation} POF_2OR + CO_2 + RF \qquad \text{(Equation 5)}$$

Combining the results from the FTIR, UV-vis, and HRMS spectra, it is clear that the free radicals generated by ionization or excitation of solvent molecules after gamma irradiation induce decomposition of $LiPF_6$ in addition to decomposition of the solvent itself. Decomposition of the electrolyte under gamma radiation causes its electrochemical performance to deteriorate, which is supported by the performance of the symmetric cell (Figure S8).

Additionally, the gamma-irradiated $LiBF_4$+EC/DEC/EMC electrolyte shows no color change, similar to that of the $LiPF_6$-based electrolyte, and no new decomposition products appeared before and after radiation, with only a difference in the content of decomposition products (Figure 2F). In other words, introduction of gamma rays into the $LiBF_4$-based electrolyte did not further trigger decomposition of $LiBF_4$, although it caused decomposition of the solvent molecules of the electrolyte. Also, the crystal structure of $LiBF_4$ did not change under gamma radiation (Figure S9). The irradiated electrolyte did not significantly affect the deposited morphology of the Li metal, so the electrochemical performance of the assembled Li||Li and Li||Cu cells remained stable, supporting good stability of the $LiBF_4$-based electrolyte against radiation (Figure S10).

PF_6^- is a stronger solvated electron scavenger than solvent molecules in $LiPF_6$-based electrolytes. Under gamma radiation, PF_6^- reacts preferentially with electrons generated by ionization to form PF_5, which further reacts with ROH/H_2O in the electrolyte to form POF_3. According to NMR investigations, the phosphorus-containing oxides formed by the interaction of POF_3 with solvent molecules or decomposition byproducts are the cause of the coloring of $LiPF_6$-based electrolytes. $LiBF_4$-based electrolytes, in contrast, exhibit strong resistance to radiation under gamma rays because the BF_4^- anion does not react with solvated and pre-solvated electrons.

Exploration of cathode active materials under gamma radiation

More comprehensive characterizations were carried out to investigate the microstructures to elucidate the deterioration mechanism of the electrochemical performance of cathode active materials under gamma radiation. The XRD spectra of LCO powders before and after gamma irradiation are displayed in Figure S11. The main peaks confirmed that both materials (LCO-0 and LCO-20) exhibit a single-phase a-$NaFeO_2$ layered structure and are indexed assuming a hexagonal-axes option of the rhombohedral R3m space group.[31] However, the cation mixing-related (003) and (104) peak intensity ratios altered dramatically, suggesting that gamma rays have an impact on the LCO crystal structure. In particular, the I_{003}/I_{104} of LCO fell from 1.96 to 1.84 after gamma radiation, indicating that the radiation exacerbated Li^+/Co^{2+} mixing.[32] Rietveld refinement patterns show that the percentages of Li^+/Co^{2+} mixing in LCO-0 and LCO-20 are 0.2% and 0.6%, respectively, and a smaller cell volume of the latter further supports damage of the LCO crystal structure by gamma radiation (Figure 3A; Tables S3 and S4).

X-ray photoelectron spectroscopy (XPS) was conducted to further confirm this conclusion. The recorded Co 2p spectra in Figure 3B were composed of Co $2p_{1/2}$ (794.8 eV) and Co $2p_{3/2}$ (779.9 eV), respectively.[33] Note that the Co^{3+} content of LCO decreased while the Co^{2+} content increased after gamma irradiation, thus triggering an escalation of Li^+/Co^{2+} mixing. In O 1s, the lattice oxygen content decreases, possibly because of the strong displacement effect of gamma rays on metal oxides (Figure S12A). The presence of adsorbed oxygen on the surface of LCO powder is attributed to the reaction of H_2O and air remaining in the argon atmosphere, and the introduction of gamma rays further accelerates the reaction between them, leading to an increase in the adsorbed oxygen content on the surface of LCO-20 (Figure S12B). As a result, the Co^{3+} in LCO may oxidize O^{2-} into O_2 and be reduced to Co^{2+} itself under gamma rays, resulting in enhancement of Li^+/Co^{2+} mixing.[29,32]

The cyclic voltammogram (CV) curves show that Li^+/Co^{2+} mixing is detrimental to the electrochemical performance of LCO (Figure S13A). The fact that LCO-20 has a weaker but more pronounced redox peak than LCO-0 indicates that it has significant electrolyte decomposition and side reactions that slow down the diffusion of Li^+. The large voltage difference between the oxidation and reduction peaks of LCO-20 indicate large polarization and poor reversibility during charging and discharging, which makes it impossible to maintain good electrochemical performance, as shown by EIS curves with a higher electrochemical impedance of LCO-20 (Figure S13B). Then, the Li^+/Co^{2+} mixing induced by gamma radiation leads to poor cycling stability and rate performance of LCO (Figure S13C).

The gamma radiation effect of LFP has also been well studied. All diffraction peaks match well with olivine LFP, as shown in XRD patterns (Figure S14).[34] The four main crystalline peaks of LFP-20 ((101), (111), (211), and (311)) are significantly lower than they were before radiation. The definite refinement in Figure 3C shows that the Fe-Li anti-site defect of LFP grew from 0.2% to 0.5% after irradiation, suggesting that gamma rays encouraged the positional exchange of Li^+ with Fe^{2+}. This was further confirmed by FTIR spectroscopy (Figure S15), where the offset value between the observed peak shift of the symmetric stretching P-O vibration peak of the PO_4 tetrahedron and the infrared absorption bands of Fe-Li defect-free in LFP at 970 cm^{-1} was utilized to evaluate the defect.[35] The results show that the P-O vibration peak of LFP under gamma radiation shifts toward the higher wavenumber region, indicating a rise in Li^+/Fe^{2+} mixing.

The composition and valence states of the surface elements further validate these results, as shown in Figure 3D. The Fe 2p spectra show two distinct peaks at binding energies of 710.3 and 723.8 eV, which are assigned to Fe $2p_{3/2}$ and Fe $2p_{1/2}$. Specifically, the decrease in Fe^{3+} content may be attributed to the fact that gamma rays promote its reaction with lattice oxygen to form Fe^{2+}, while the increase in Fe^{2+} content exacerbates Li^+/Fe^{2+} mixing. In addition, the decrease of the lattice oxygen content in the O 1s spectrum under gamma radiation confirms this possibility (Figure S16).

Blocking of the one-dimension channel by Li^+/Fe^{2+} mixing would lead to a deterioration of the Li^+ diffusion pathway. The CV curve test shows that the gamma-irradiated LFP exhibits a large potential difference during charge and discharge, indicating large Li^+ diffusion polarization and poor reversibility (Figure S17A). The EIS test further confirms that Li^+/Fe^{2+} mixing causes the deteriorated charge transfer kinetics of LFP (Figure S17B). Based on this, the capacity and rate performance of the irradiated LFP gradually deteriorated as the rate increased from 0.5 to 10 C, and the reversible capacity could not be recovered (Figure S17C).

Gamma radiation also had an impact on the structure of NCM811. The layered α-$NaFeO_2$ structure (R3m) is indicated by the XRD patterns of the NCM811-0 and
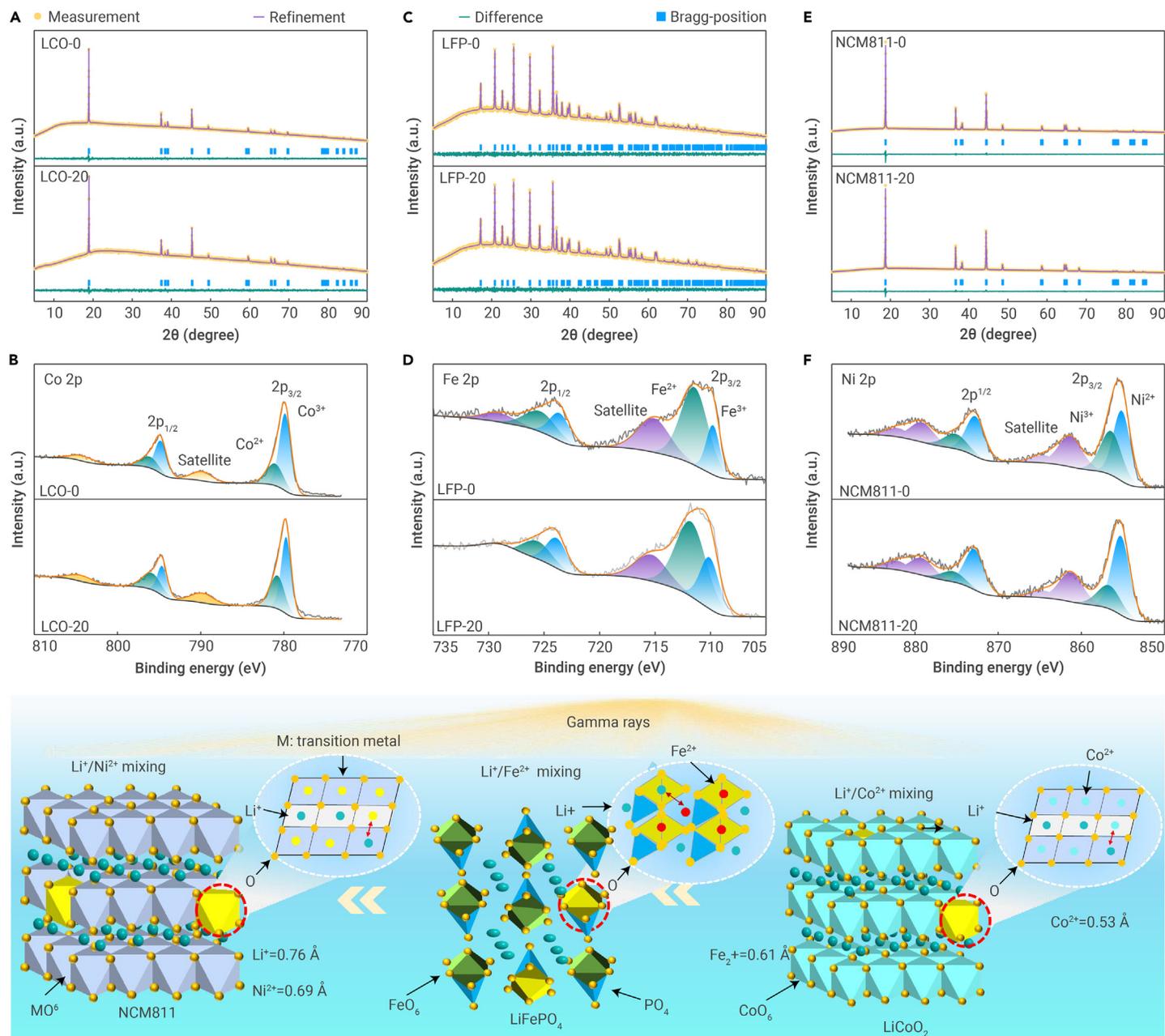
Figure 3. Exploration of cathode active materials under gamma radiation (A and B) Rietveld refinement results of (A) XRD patterns and high-resolution (B) XPS Co 2p spectra for LCO. (C and D) Rietveld refinement results of (C) XRD patterns and high-resolution (D) XPS Fe 2p spectra for LFP. (E and F) Rietveld refinement results of (E) XRD patterns and (F) high-resolution XPS Co 2p spectra for NCM811. (G) Deterioration mechanism of cathode materials under gamma irradiation.

NCM811-20 samples, suggesting that gamma radiation has no effect on the layered structure.[36] The I_{003}/I_{104} intensity ratio of NCM811-0 (1.80) is slightly higher than that of NCM811-20 (1.76), indicating a slight increase in Li^+/Ni^{2+} mixing under gamma radiation (Figure S18). The crystal structures were further examined by Rietveld refinements (Figure 3E). The unit cell volume of NCM811-20 is slightly reduced in comparison with that of NCM811-0, indicating gamma-induced mixing of Li^+ with Ni^{2+}. That is, gamma radiation contributes to increasing the degree of Li^+/Ni^{2+} mixing because the occupancy of Ni^{2+} in the Li site of NCM811-20 (0.95%) is slightly higher than that of NCM811-0 (0.7%). Moreover, the XPS Ni 2p spectra of NCM811-0 and NCM811-20 verify the existence of Ni^{2+} with typical peaks at 854.8 and 860.9 eV and Ni^{3+} at binding energies of 856.3 and 864.2 eV (Figure 3F).[37] Compared with NCM811-0, the introduction of gamma rays decreased the Ni^{3+} content and increased Ni^{2+}, leading to increased mixing of Li^+ with Ni^{2+}. The conversion of Ni^{3+} to Ni^{2+} catalyzed by gamma rays in the presence of oxygen could be the cause of the drop in Ni^{3+} content. The O 1s spectra provide direct evidence of the reduction of the lattice oxygen content in NCM811-20 (Figure S19A). Simultaneously, the introduction of

gamma rays accelerated the reaction between NCM811 and the remaining air in the argon atmosphere, resulting in an increase in Li_2CO_3 content, which is detrimental to the enhancement of electrochemical performance (Figure S19B).

Li^+/Ni^{2+} mixing is also detrimental to the electrochemical performance of NCM811. According to the CV curves of NCM811-0 and NCM811-20 (Figure S20A), oxidation of Ni^{2+} to Ni^{3+}/Ni^{4+} is represented by the oxidation peaks in the voltage range of 3.6–4.0 V, while oxidation of Co^{3+} to Co^{4+} is shown at 4.2 V.[38] The NCM811-20 redox peak seems faint and broad, indicating poor ion transport kinetics of Li^+/Ni^{2+} mixing. The potential difference of NCM811-20 is also greater than that of NCM811-0, which also supports the idea that gamma ray-induced ion mixing worsens the electrochemical characteristics by increasing polarization. A larger electrochemical impedance of NCM811-20 than NCM811-0 in electrochemical impedance spectroscopy (EIS) spectra further confirms the effect of Li^+/Ni^{2+} mixing on cell polarization (Figure S20B). The rate performance demonstrates that Li^+/Ni^{2+} mixing obstructs Li^+ transport, preventing some Li^+ from being buried in the lattice, leading to a lower reversible capacity and a shorter cycle life (Figure S20C).
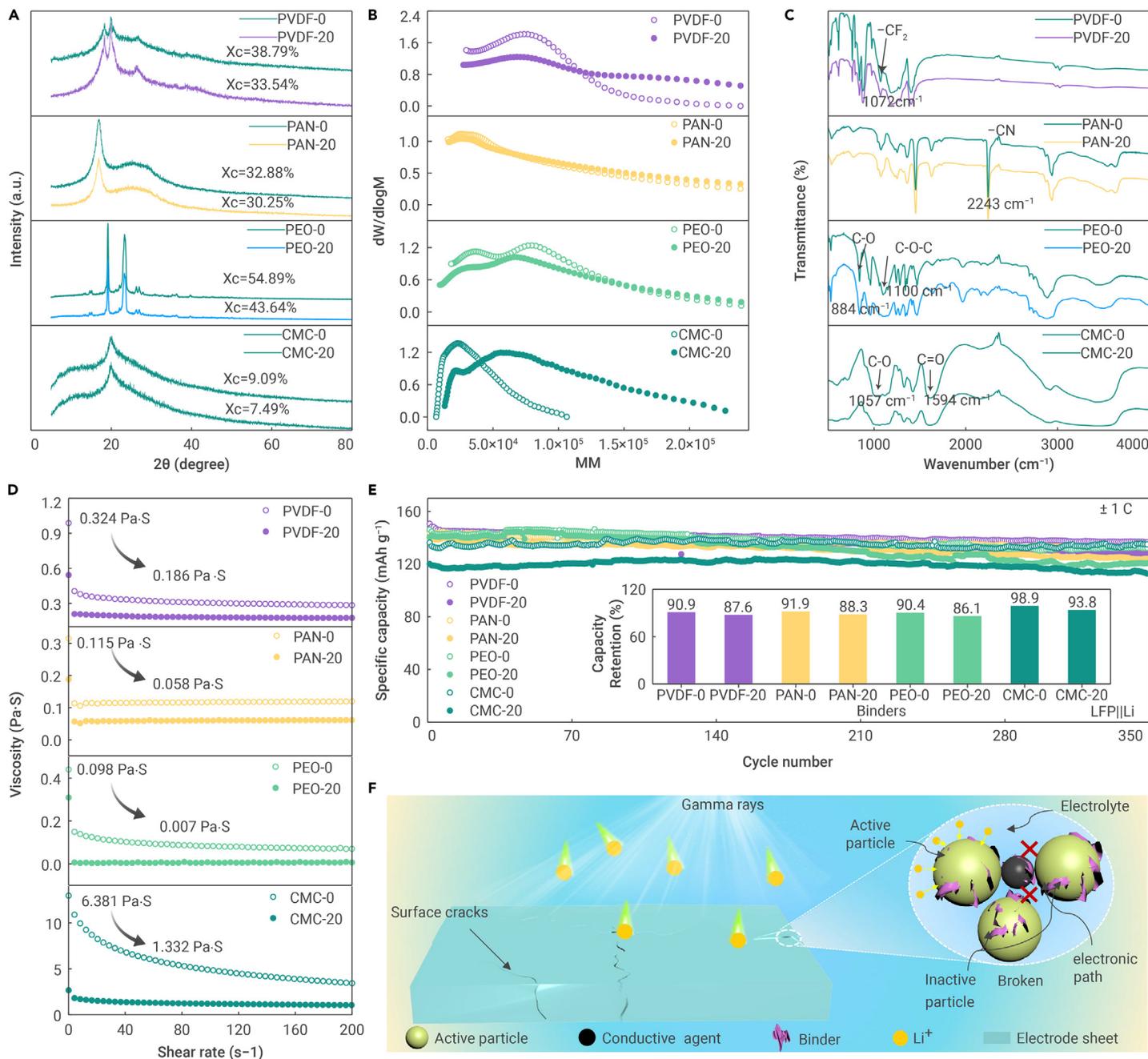
Figure 4. Electrochemical analysis of binders under gamma radiation (A–D) XRD patterns(A), M_M curves (B), FTIR spectra (C), and viscosity curves (D) of the binders before and after gamma irradiation. (E) Cycling performance of LFP||Li batteries with different binders. The inset shows a comparison of the capacity retention rates of LFP||Li batteries based on four binders after 350 cycles. (F) Mechanism of binder-induced deterioration of battery performance under gamma radiation.

The Li$^+$ on the lattice sites of active cathode materials may absorb the energy of gamma radiation, which speeds up their wagging vibration and intensifies the disordering of the structure. The Li$^+$/Ni^{2+}, Li$^+$/Fe^{2+}, and Li$^+$/Co^{2+} mixing that enhanced cell polarization and led to poor reversible capacity and cycle life should be responsible for the deteriorated electrochemical performance of NCM811, LFP, and LCO materials under gamma radiation (Figure 3G). The radiation tolerance of the three cathode materials follows the order of NCM811, LFP, and LCO, and this performance difference is assigned to the formation energy of cation mixing. The most easily created defect in metal oxides during radiation is the cation anti-site defect, and the lower the cation anti-site defect energy, the greater the radiation tolerance.[39] It has been demonstrated that the cation anti-site defect energy decreases with decreasing cation radius ratio, and the associated radiation tolerance improves.[40] The cation radius ratios in NCM811, LFP, and LCO are in the sequence of Li$^+$/Ni^{2+} < Li$^+$/Fe^{2+} < Li$^+$/Co^{2+}, and as a result, their radiation tolerance follows NCM811 > LFP >

LCO, which is consistent with the abovementioned changes in electrochemical performance and crystal structures.

Electrochemical analysis of binders under gamma radiation

Molecular-level changes in the binder were carefully investigated to elucidate the intrinsic mechanism of binder-induced deterioration of battery performance under gamma radiation. Various common binders, including CMC, PEO, and PAN, were examined to offer recommendations for the choice of binders in future radiation environments. Figure 4A shows the XRD patterns of the PVDF, PAN, PEO, and CMC binders before and after gamma irradiation. After irradiation, the crystallinity of the four binders drastically diminished, demonstrating that gamma radiation induced chain breaking and cross-linking of the binder molecules. Moreover, the molecular weight distribution curves of the four binders, as shown in Figure 4B, exhibit a weak peak in the low-molecular-weight region after radiation. This is because gamma radiation induces the binder molecules to break their chains, reducing the number of binder molecules. Similarly, the
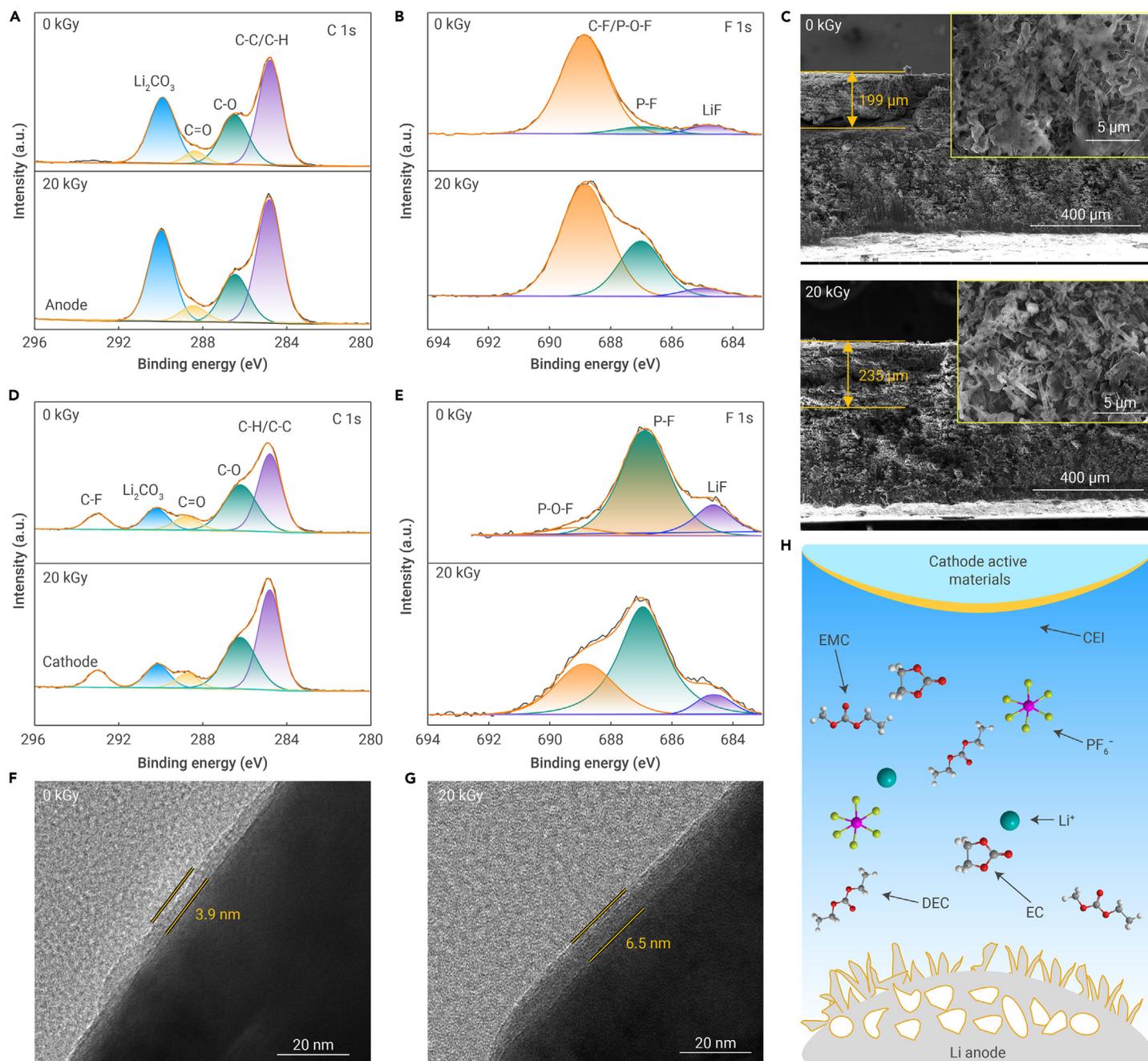
Figure 5. Interface chemistry of Li metal batteries under gamma radiation (A and B) XPS O 1s (A) and F 1s (B) spectra of SEI on the Li metal anode surface after 100 cycles. (C) SEM images of the Li metal anode after 100 cycles. (D and E) XPS O 1s (D) and F 1s (E) spectra of CEI on the NCM811 cathode surface after 100 cycles. (F and G) Transmission electron microscopy (TEM) images of the NCM811 cathode after 100 cycles (F) before and (G) after radiation. (H) Interfacial deterioration mechanisms of Li metal batteries under gamma radiation.

peak intensification in the high-molecular-weight region indicates that gamma radiation promotes the cross-linking reaction of binder molecules, driving an increase in binder molecular content. In particular, a heavy average molecular mass (M_M) comparison shows that the M_M of the PVDF, PAN, and CMC binders increases after irradiation, showing that the three are primarily cross-linked under gamma radiation (Table S9). PEO molecules, on the other hand, are more likely to break chains when exposed to gamma radiation because of their high crystallinity and flexible molecular chains.

FTIR spectra provide insight into the microstructural transformations of the binder molecules under gamma radiation (Figure 4C). The peaks at 613, 761, 796, 972, 1,205, and 1,384 cm^{-1} for PVDF demonstrate that no new peaks occur after gamma irradiation, namely that still preserve the α-phase.[41] However, the characteristic peak of $-CF_2$ (1,071 cm^{-1}) decreases after irradiation, indicating that the gamma rays destroy the polar functional groups of PVDF molecules, which is detrimental to the maintenance of its bonding ability. For PAN, gamma

radiation also destroys its polar functional group ($-CN$, 2,243 cm^{-1}), showing a weak absorption peak.[42] For PEO, the polar functional groups of $C-O$ (884 cm^{-1}) and $C-O-C$ (1100 cm^{-1}) decrease after radiation, indicating that the polymer chain breaking and cross-linking are caused by gamma radiation.[43] For CMC, the FTIR spectrum of CMC-20 also shows a decrease in characteristic peaks, like $C-O$ (1,057 cm^{-1}) and $C=O$ (1,594 cm^{-1}).[44]

The variation in the content of polar functional groups in the binder molecules has a vital effect on their bonding ability. The viscosity curves confirm that the PVDF, PAN, PEO, and CMC binders decline substantially after gamma irradiation, with the last one declining the most (Figure 4D). The decrease in bonding ability of the binders leads to poor electron-ion conductivity between the carriers (active material and conductive agent) in the cathode, triggering large cell polarization (Figure S21). Further, the side effects were amplified after 100 cycles, and the volume expansion led to cracks on the surface of the electrode (Figure S22). The low active material utilization and large polarization make the electrochemical
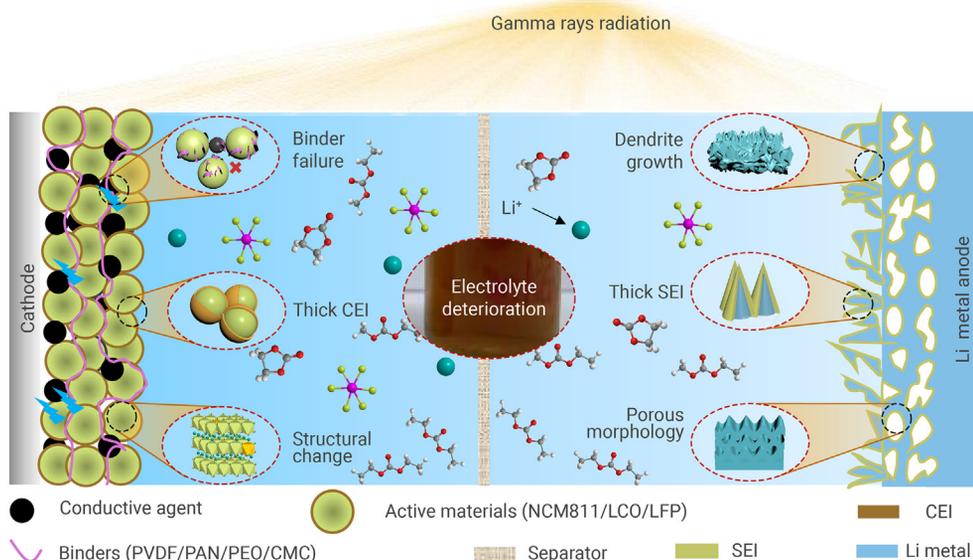
Figure 6. Deterioration mechanism of Li metal batteries under gamma radiation

from the fact that decomposition of the electrolyte directly enhances its reactivity with Li metal.

According to Figures 5D and 5E, the NCM811 cathode electrolyte interphase (CEI) component changes in a manner similar to the Li metal anode's. The rapid embedding and detachment of Li^+ on the cathode side is hindered by the NCM811 cathode surface's increased CEI thickness under gamma radiation, which rises from 3.9 to 6.5 nm (Figures 5F and 5G). Along with the degradation of the cathode active material and electrolyte, the binder also deteriorates, which increases the interfacial reaction on the cathode. The deterioration of the bonding ability of the binder causes cracks in the electrode, which further enhances the electrolyte-cathode side reaction.

The effect of gamma radiation on the interface between the cathode and anode in Li metal batteries deteriorates the ion transport kinetic behavior. As shown in Figure S26, the R_b and R_{ct} of Li metal batteries significantly increase under gamma radiation. The former is attributed to the decomposition effect of gamma rays on $LiPF_6$ and solvent, which intensifies their parasitic reactions with Li metal and leads to low ionic conductivity. Also, the latter is responsible for the abundant organic components in the interface chemistry of the electrode. In short, the destructive effects of gamma radiation on the key materials (cathode active material, binder, and electrolyte) in Li metal batteries synergistically deteriorate the interface between the cathode and anode, leading to a series of problems (Figure 5H). Specifically, the deterioration of the interface on the Li anode cannot effectively regulate the uniform deposition of Li^+ and aggravates the occurrence of dendrites and side reactions. The deterioration of the cathode interface exacerbates the side reactions of the electrolyte and active material, leading to formation of a thick CEI layer.

performance of the battery deteriorate. Specifically, the capacity retention of LFP|| Li batteries using PVDF-20, PAN-20, PEO-20, and CMC-20 after 350 cycles at 1 C rate were 87.6%, 88.3%, 86.1%, and 93.8%, respectively, compared with 90.9%, 91.9%, 90.4%, and 98.9% for the control group (Figure 4E). Also, the irradiated binder made the rate performance of the LFP||Li batteries worse (Figure S23).

According to the aforementioned investigation, the radiation tolerance of the four binders under gamma radiation follows the order PVDF > PAN > PEO > CMC. The failure of Li metal batteries is mainly attributed to the decrease in bonding ability because of the change in binder molecular structure, which leads to low active material utilization and large cell polarization, thus deteriorating the electrochemical performance of Li metal batteries (Figure 4F). Under gamma radiation, the chain breaking and cross-linking reactions of binder molecules occur simultaneously, with the former being dominated by more end groups in the molecule and low crystallinity and the latter being dominated by high molecular chain flexibility and high crystallinity. The results suggest that PVDF is more adaptive to radiation environment applications compared with other binders.

Interface chemistry of Li metal batteries under gamma radiation

To understand the derived side effects triggered by deterioration of the above key materials (i.e., cathode active materials, binder, and electrolyte), the interface chemistry of Li metal batteries was further explored under gamma radiation. Note that the NCM811 cathode and Li metal anode in NCM811||Li batteries with 100 cycles at 1 C rate were collected for XPS testing. Figure 5A shows recorded C 1s for the Li metal anode before and after radiation, which are assigned to C−C/C−H (284.7 eV), C−O (285.5 eV), C=O (286.6 eV), and Li_2CO_3 (290.1 eV).[45] Apparently, the organic components and Li_2CO_3 content on the Li metal anode surface increased because of the intensified side reactions between the electrolyte and Li metal after gamma radiation. The F 1s originating from decomposition of $LiPF_6$ was fitted to LiF (684.9 eV), P−F (687.1 eV), and P−O−F (688.9 eV) (Figure 5B).[46] The P−O−F content on the surface of Li metal increased because of destruction of $LiPF_6$ by gamma radiation, which is compatible with the findings in the P 2p spectrum (Figure S24). In addition, the mechanical strength of the SEI on the surface of the Li metal anode confirms the effect of gamma radiation on electrolyte decomposition, resulting in a low Young's modulus (Figure S25). The continuous decomposition of $LiPF_6$ decreases the ionic conductivity of the electrolyte and increases cell polarization. Simultaneously, the deteriorated SEI on the surface of the Li metal anode is not conducive to uniform deposition of Li^+, which triggers the crazy growth of dendrites and damage to the Li substrate, as shown by poor electrode morphology (Figure 5C). Compared with conventional conditions, the Li metal anode shows a more sparse and porous dendrite morphology under gamma radiation, and the thickness of the "dead Li" layer reaches 235 μm. Apparently, gamma radiation also indirectly accelerates failure of the Li metal anode, which, on one hand, stems from the fact that the cation mixing of the cathode active material intensifies the dissolution of the transition metal ions and catalyzes the interfacial reaction at the anode and, on the other hand, derives

Deterioration mechanism of Li metal batteries under gamma radiation

Based on the above analysis, the cathode active material, binder, electrolyte, and electrode interface are responsible for degradation of the electrochemical performance of Li metal batteries when exposed to gamma radiation (Figure 6). In particular, gamma radiation causes Li^+/Ni^{2+}, Li^+/Co^{2+}, and Li^+/Fe^{2+} mixing in NCM811, LCO, and LFP materials, respectively, which enhances ion transport hindrance and leads to poor reversible capacity and cycle life. For the binder, the chain breaking and cross-linking of the binder molecules by gamma radiation reduces the bonding ability, driving cracking of the electrode and lower utilization of the active material, which leads to poor reversible capacity and cycle life. For electrolyte, the free radicals generated by ionization of solvent molecules under gamma radiation cause decomposition of $LiPF_6$, leading to deterioration of the electrolyte's performance. For the electrode interface, the degradation of SEI causes dendrites and "dead Li" to hasten the quick failure of the Li metal anode for one thing, and for another, the degradation of CEI also amplifies the interfacial side reactions to increase polarization. As a result, Li metal batteries show poor electrochemical performance under gamma radiation.

CONCLUSION

In summary, this work innovatively considers gamma rays for Li metal batteries and reveals the intrinsic mechanism of performance deterioration. With no discernible impact on the separator, conductive agent, or Li metal, the electrolyte, cathode active material, and binder are mostly responsible for the electrochemical performance degradation of Li metal batteries under gamma radiation and follow this order. More specifically, gamma radiation triggers cation mixing in the cathode active material, which increases cell polarization and leads to poor reversible capacity and cycle life. Compared with LCO and LFP, the high-capacity NCM811 cathode material possesses the best stability against radiation because of the smaller cation radius difference. Further, chain breaking and

cross-linking of binder molecules under gamma radiation reduces their bonding ability, which makes the electrode sheet crack and reduces active material utilization, further aggravating the deterioration of battery performance. Among the four popular binders (PVDF, PAN, CMC, and PEO), PVDF possesses the best irradiation tolerance. Ionization of solvent molecules under gamma radiation induces decomposition of $LiPF_6$ along with its own decomposition, which further aggravates the deterioration of battery performance. Compared with $LiPF_6$, $LiBF_4$-based electrolytes have better stability against radiation. Failure of the cathode active material, binder, and electrolyte in Li metal batteries further deteriorates the interface chemistry of the cathode and anode, prompting rapid failure of the Li metal anode and an increase in cell polarization, which then further accelerates deterioration of the electrochemical performance of Li metal batteries. This analysis shows that choosing materials (cathode active material, binder, and electrolyte) with better radiation tolerance as battery materials can greatly mitigate deterioration of performance in a radiation environment. A further option for enhancing the radiation tolerance of the battery is application of radiation-resistant coatings (such as metal oxide or nanostructure composite coatings) to the surfaces of the cell, electrode, or materials.

MATERIALS AND METHODS

See supplemental information for details.

REFERENCES

1. Liu, D.,H., Bai, Z., Li, M., et al. (2020). Developing high safety Li-metal anodes for future high-energy Li-metal batteries: strategies and perspectives. Chem. Soc. Rev. **49**, 5407–5445.
2. Li, J., Ho, M.S., Xie, C., et al. (2022). China's flexibility challenge in achieving carbon neutrality by 2060. Renew. Sustain. Energy Rev. **158**, 112112.
3. Niu, C., Liu, D., Lochala, J.A., et al. (2021). Balancing interfacial reactions to achieve long cycle life in high-energy lithium metal batteries. Nat. Energy **6**, 723–732.
4. Xu, R., Cheng, X.-B., Yan, C., et al. (2019). Artificial interphases for highly stable lithium metal anode. Matter **1**, 317–344.
5. Gao, M., Li, H., Xu, L., et al. (2021). Lithium metal batteries for high energy density: Fundamental electrochemistry and challenges. J. Energy Chem. **59**, 666–687.
6. Li, Z., Peng, M., Zhou, X., et al. (2021). In situ chemical lithiation transforms diamond-like carbon into an ultrastrong ion conductor for dendrite-free lithium-metal anodes. Adv. Mater. **33**, e2100793.
7. Li, X., Yuan, L., Liu, D., et al. (2021). Elevated lithium ion regulation by a "natural silk" modified separator for high-performance lithium metal anode. Adv. Funct. Mater. **31**, 2100537.
8. Zhao, Q., Wang, R., Hu, X., et al. (2022). Functionalized 12 micron polyethylene separator to realize dendrite-free lithium deposition toward highly stable lithium-metal batteries. Adv. Sci. **9**, e2102215.
9. Luo, D., Li, M., Zheng, Y., et al. (2021). Electrolyte design for lithium metal anode-based batteries toward extreme temperature application. Adv. Sci. **8**, e2101051.
10. Kim, M.S., Zhang, Z., Rudnicki, P.E., et al. (2022). Suspension electrolyte with modified Li^+ solvation environment for lithium metal batteries. Nat. Mater. **21**, 445–454.
11. Zhu, C., Sun, C., Li, R., et al. (2022). Anion-diluent pairing for stable high-energy Li metal batteries. ACS Energy Lett. **7**, 1338–1347.
12. Jain, R., Lakhnot, A.S., Bhimani, K., et al. (2022). Nanostructuring versus microstructuring in battery electrodes. Nat. Rev. Mater. **7**, 736–746.
13. Chen, H., Yang, Y., Boyle, D.T., et al. (2021). Free-standing ultrathin lithium metal-graphene oxide host foils with controllable thickness for lithium batteries. Nat. Energy **6**, 790–798.
14. Ju, Z., Lu, G., Sheng, O., et al. (2022). Soybean protein fiber enabled controllable Li deposition and a LiF-nanocrystal-enriched interface for stable Li metal batteries. Nano Lett. **22**, 1374–1381.
15. Gao, Y., Guo, M., Yuan, K., et al. (2019). Multifunctional silanization interface for high-energy and low-gassing lithium metal pouch cells. Adv. Energy Mater. **10**, 1903362.
16. Guo, W., Han, Q., Jiao, J., et al. (2021). In situ construction of robust biphasic surface layers on lithium metal for lithium-sulfide batteries with long cycle life. Angew. Chem. Int. Ed. **60**, 7267–7274.
17. Li, S., Huang, J., Cui, Y., et al. (2022). A robust all-organic protective layer towards ultrahigh-rate and large-capacity Li metal anodes. Nat. Nanotechnol. **17**, 613–621.
18. Gao, Y., Qiao, F., You, J., et al. (2022). Effect of the supergravity on the formation and cycle life of non-aqueous lithium metal batteries. Nat. Commun. **13**, 5.
19. Chen, M., Wang, C., and Hu, W. (2021). Organic photoelectric materials for X-ray and gamma ray detection: mechanism, material preparation and application. J. Mater. Chem. C **9**, 4709–4729.
20. Rahman, M.M., Chen, W.-Y., Mu, L., et al. (2020). Defect and structural evolution under high-energy ion irradiation informs battery materials design for extreme environments. Nat. Commun. **11**, 4548.
21. Rouif, S. (2005). Radiation cross-linked polymers: Recent developments and new applications. Nucl. Instrum. Meth B **236**, 68–72.
22. Polf, J.C., and Parodi, K. (2015). Imaging particle beams for cancer treatment. Phys. Today **68**, 28–33.
23. Qu, Y., Jin, S., Zhang, A., et al. (2010). Gamma-ray resistance of regulatory $CD4^+CD25^+Foxp3^+$ T cells in mice. Radiat. Res. **173**, 148–157.
24. Dong, C., He, M., Tu, W., et al. (2015). The differential role of human macrophage in triggering secondary bystander effects after either gamma-ray or carbon beam irradiation. Cancer Lett. **363**, 92–100.
25. Onoda, S., Mori, H., Okamoto, T., et al. (2001). Investigation of radiation degradation of Si and GaAlAs optical devices due to gamma-ray and electron irradiation. Radiat. Phys. Chem. **60**, 377–380.
26. Lezius, M., Predehl, K., Stöwer, W., et al. (2012). Radiation induced absorption in rare earth doped optical fibers. IEEE T. Nucl. Sci. **59**, 425–433.
27. Gorelick, J.L., Ladbury, R., and Ka, L. (2004). The effects of neutron irradiation on gamma sensitivity of linear integrated circuits. IEEE Trans. Nucl. Sci. **51**, 3679–3685.
28. Wang, C., Sun, Y., Cao, G., et al. (2015). Radiation dose evaluation and analysis inside FY-3A satellite. J. Space Science **35**, 56–63.
29. Ding, N., Zhu, J., Yao, Y., et al. (2006). The effects of gamma-radiation on lithium-ion cells. Electrochim. Acta **51**, 6320–6324.
30. Tan, C., Lyons, D.J., Pan, K., et al. (2016). Radiation effects on the electrode and electrolyte of a lithium-ion battery. J. Power Sources **318**, 242–250.
31. He, S., Wei, A., Li, W., et al. (2019). Al-Ti-oxide coated $LiCoO_2$ cathode material with enhanced electrochemical performance at a high cutoff charge potential of 4.5 V. J. Alloys Compd. **799**, 137–146.
32. Ding, N., Zhu, J., Yao, Y., et al. (2006). The effects of γ-radiation on $LiCoO_2$. Chem. Phys. Lett. **426**, 324–328.
33. Chen, G., Geng, H., Wang, Z., et al. (2015). On electrochemistry of Al_2O_3-coated $LiCoO_2$ composite cathode with improved cycle stability. Ionics **22**, 629–636.
34. Wang, H., Chen, W., Li, D., et al. (2017). In-situ self-polymerization restriction to form core-shell $LiFePO_4$/C nanocomposite with ultrafast rate capability for high-power Li-ion batteries. Aging Dis. **8**, 346–353.
35. Zou, Y., Chen, S., Yang, X., et al. (2016). Suppressing Fe-Li antisite defects in $LiFePO_4$/carbon hybrid microtube to enhance the lithium ion storage. Adv. Energy Mater. **6**, 1601549.
36. Ran, Q., Zhao, H., Hu, Y., et al. (2020). Multifunctional integration of double-shell hybrid nanostructure for alleviating surface degradation of $LiNi_{0.8}Co_{0.1}Mn_{0.1}O_2$ cathode for advanced lithium-ion batteries at high cutoff voltage. ACS Appl. Mater. Interfaces **12**, 9268–9276.
37. Han, Q., Sha, W., He, J., et al. (2022). Modification of $LiNi_{0.8}Co_{0.1}Mn_{0.1}$ cathode with Al-Screened $LiPO_3$ to enhance interfacial stability and ionic dynamics. Chem. Eng. J. **446**, 137051.
38. Rn, R., Bosubabu, D., Mg, K.B., et al. (2020). Tuning of Ni, Mn, and Co (NMC) content in $0.4(LiNi_xMn_yCo_zO_2)0.4(Li_2MnO_3)$ toward stable high-capacity lithium-rich cathode materials. ACS Appl. Energy Mater. **3**, 10872–10881.
39. Sickafus, K.E., Minervini, L., Grimes, R.W., et al. (2000). Radiation tolerance of complex oxides. Science **289**, 748–751.
40. Begg, B.D., Hess, N.J., McCready, D.E., et al. (2001). Heavy-ion irradiation effects in $Gd_2(Ti_{2-x}Zr_x)O_7$ pyrochlores. J. Nucl. Mater. **289**, 188–193.
41. Babu, K.F., and Choi, W.M. (2016). Thermal actuation properties of bimorph based on PVDF/rGO composites. Compos. Sci. Technol. **122**, 82–89.
42. Jyothi, N.K., Kumar, K.V., and Murthy, P.N. (2014). FTIR, XRD and DC conductivity studies of proton conducting gel polymer electrolytes based on polyacrylonitrile (PAN). Int. J. ChemTech Res. **6**, 5214–5219.
43. Chandrasekaran, R., Ruth Mangani, I., Selladurai, S., et al. (2001). Ionic conductivity and battery characteristic studies on $PEO+NaClO_3$ polymer electrolyte. Ionics **7**, 88–93.
44. Ahmad, N.H., and Isa, M. (2015). Structural and ionic conductivity studies of CMC based polymerelectrolyte doped with NH_4Cl. Adv. Mat. Res. **1107**, 247–252.
45. Liu, F., Zhang, Z., Yu, Z., et al. (2022). Bifunctional nitrile-borate based electrolyte additive enables excellent electrochemical stability of lithium metal batteries with single-crystal Ni-rich cathode at 4.7 V. Chem. Eng. J. **434**, 134745.
46. Fang, S., Zhang, Y., and Liu, X. (2021). Lithium anode in carbonate-based electrolyte: High-performance by self-protected solid-electrolyte-interphase. Chem. Eng. J. **426**, 131880.

ACKNOWLEDGMENTS

AUTHOR CONTRIBUTIONS

K.X. and Y.G. conceived the idea. Y.G. and F.Q. performed major experiments. W.H., L.M., C.S., and T.J. provided some electrochemical characterizations. Y.G. wrote the draft. N.L. and K.X. revised the paper as well as supervised the research. All authors participated in analyzing the experimental results and preparing the manuscript.

DECLARATION OF INTERESTS

The authors declare no competing interests.

SUPPLEMENTAL INFORMATION

It can be found online at https://doi.org/10.1016/j.xinn.2023.100468.

LEAD CONTACT WEBSITE

Keyu Xie, https://teacher.nwpu.edu.cn/xiekeyu.html.